Environ. Sci. Technol. **1998**, *32,* 943−955

Rock−Water Interactions Controlling Zinc, Cadmium, and Lead Concentrations in Surface Waters and Sediments, U.S. Tri-State Mining District. 1. Molecular Identification Using X-ray Absorption Spectroscopy

PEGGY A. O'DAY,*,† SUSAN A. CARROLL,‡ AND GLENN A. WAYCHUNAS§

Department of Geology, Arizona State University, Tempe, Arizona 85287-1404, Earth and Environmental Sciences Directorate, Lawrence Livermore National Laboratory, Livermore, California 94551, and Center for Materials Research, Stanford University, Stanford, California 94305

X-ray absorption spectroscopy (XAS) and X-ray absorption fine structure (XAFS) spectra of zinc-, cadmium-, and lead-bearing sediments from a mining-impacted site in the U.S. Tri-State Mining District (Kansas−Missouri−Oklahoma) are used to identify the local molecular coordination of metals in contaminated, untreated stream sediments. Quantitative analysis of the XAFS spectra, supplemented by elemental distributions on particles provided by electron microprobe and secondary ion mass spectrometry (SIMS), shows that zinc and cadmium occur in small (<1 μm), residual particles of the host ore, sphalerite (ZnS) in which cadmium substitutes for zinc in the mineral structure. In half of the samples studied, analyses indicate that zinc, as it weathers from sphalerite, is scavenged primarily by zinc hydroxide and/or zinc−iron oxyhydroxide phases, depending on the total amount of iron in the system. These phases probably form as amorphous or poorly crystalline coatings on mineral surfaces. There is no evidence that zinc sorption or substitution in other mineral phases is a significant mode of uptake. In contrast, there is no spectral evidence for the association of cadmium with secondary oxide or oxyhydroxide phases in both high- and low-iron samples. Cadmium bound in sphalerite is found in all samples; evidence for cadmium uptake into a carbonate phase (in addition to sphalerite) is found in only one sample. This result may suggest preferential partitioning of cadmium, relative to zinc, into the aqueous phase as sphalerite weathers. XAFS spectra of lead in sediments with low total iron concentrations indicate no evidence for Pb bonding in galena (PbS), the host ore, and suggest lead uptake in secondary carbonate and/or oxide phases. Uptake of metal ions from solution into secondary phases is apparently governed by competition between iron oxyhydroxide and carbonate phases that can be related to total iron in the sediments and to stream pH. This work highlights the differential chemical behavior of three divalent metal cations in a contaminated system and demonstrates the need for direct molecular identification of metal coordination in order to generate accurate geochemical predictions.

Introduction

The contamination of surface waters, groundwater, soils, and sediments by hazardous trace metals is a widespread environmental problem resulting from mining activities and industrial discharges. Accurate chemical modeling of metal transport and partitioning in these complex, multicomponent systems requires direct knowledge of how metals are sequestered by natural solid phases. These solids are complicated mixtures of weathered primary minerals and crystalline and amorphous secondary phases that precipitate from coexisting waters. Hazard assessment and remediation in complex systems are often difficult because few spectroscopic probes are specific and sensitive enough to provide bonding information about individual metals at low bulk concentrations. Synchrotron radiation X-ray absorption spectroscopy (XAS) is useful for determining the local bonding of metal ions in natural soils and sediments. This technique has the advantages of relatively high sensitivity (in the range of 10's to 1000's of ppm) for elements of $Z > 20$ under nonvacuum conditions and the ability to probe the local atomic bonding of a specific element in amorphous and disordered phases that are typical of natural systems (*1*).

In this study, we use XAS and quantitative analysis of the X-ray absorption fine structure (XAFS) to obtain structural information about the local atomic coordination of trace zinc, cadmium, and lead in untreated stream sediment samples from a mine drainage area in the U.S. Tri-State Mining District (Kansas−Missouri−Oklahoma). We supplement XAFS data from bulk samples with imaging and elemental mapping using electron microprobe (EM) and secondary ion mass spectrometry (SIMS) to obtain information about the spatial distribution of these elements. Together, these techniques provide molecular-to-micrometer-scale identification of the primary solid phases associated with these three metals. In a companion paper by Carroll et al. (*2*), the solid-phase constraints from spectroscopy and microscopy are coupled with thermodynamic calculations of aqueous speciation and mineral saturation state to assess the geochemical reactions that govern the fate and transport of metals in this contaminated system.

Application of XAS to Natural Sediments. Synchrotron radiation spectroscopies such as X-ray absorption spectroscopy (XAS) and its derivatives, X-ray absorption fine structure (XAFS) and X-ray absorption near-edge structure (XANES) spectroscopy, are emerging as powerful tools for the study of trace elements in natural materials. The high photon flux afforded by synchrotron radiation enables examination of elements at orders of magnitude lower concentrations than conventional laboratory X-ray sources. The tunability of synchrotron light over a broad energy spectrum allows element-specific spectral analysis that can supply quantitative interatomic bond distances (usually $\pm 0.01-0.03$ Å) between absorber and backscatterer atoms and information about the identity and coordination of near-neighbor atoms, with

* To whom correspondence should be addressed: voice: (602) 965−4581; fax: (602) 965-8102; e-mail: oday@asu.edu.
† Arizona State University.
‡ Lawrence Livermore National Laboratory.
§ Stanford University.

S0013-936X(97)00453-7 CCC: $15.00
Published on Web 02/28/1998

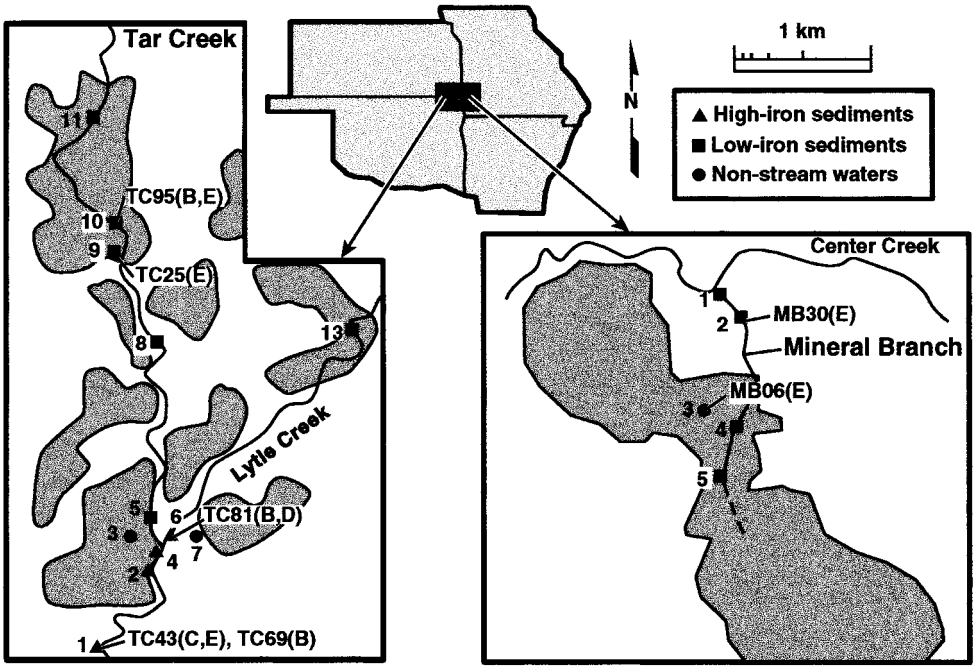

FIGURE 1. Location of stream sediments in the Tri-State Mining District analyzed by XAS. Shaded areas are tailings piles; numbers indicate streamwater sampling sites (see ref 2, for analyses of water chemistry).

or without an aqueous phase present (*3, 4*). This information can be used to identify the speciation and coordination site of the element of interest in the solid or liquid phase. To date, the majority of XAS studies of metal sorption and precipitation have examined model systems composed of a single metal ion and pure mineral substrates, either powder or single crystal (see reviews in refs 1 and 5). Fewer more recent studies have applied XAS directly to complicated natural materials such as soils and sediments (*6*−*9*).

There are a number of experimental challenges that arise in applying XAS directly to the study of natural samples. An X-ray absorption spectrum from a bulk, powdered sample gives an average bonding environment for the atom of interest. Thus, if an atom exists in more than one bonding site, the absorption spectrum will be a weighted average of all sites. In simple mixtures of two distinct atomic sites, mixing can usually be quantified with the aid of known reference compounds. In more complicated mixtures or for sites with high static disorder, either an average of all bond lengths or biasing toward shorter bond lengths (when atomic vibrations are anharmonic) are derived from least-squares fits (*10*). Thus, the spectral interpretation can be complicated without a sufficient number of known reference compounds for comparison or without independent confirmation from a complementary analytical technique. Data collection at liquid He temperature (≈10 K) for dry samples significantly improves signal-to-noise, reduces atomic vibrations, and allows better quantification of near-neighbor backscatterers. For wet or dry samples at room temperature, spectral features beyond the first coordination shell have significantly lower amplitude than those in low-temperature spectra, and their quantification and interpretation must be done with caution. In using XAS on bulk samples, it must be kept in mind that metal coordination in minor phases, anything less than about 10 atom %, will probably not be distinguishable in the absorption spectrum.

In this study, our approach was to use quantitative XAS as a means to distinguish the primary phases coordinating the metals present in these sediments (e.g., distinguishing among metal coordination in oxide, sulfide, sulfate, or carbonate phases). This information is obtained primarily by using first and higher shell interatomic bond distances as "fingerprints" indicative of the primary site(s) of metal coordination. In samples where there are mixtures of phases, the spectral amplitude (and thus the fitted coordination numbers and values for the disorder parameter, σ^2) will reflect relative proportions of the mixture rather than the expected atomic coordination numbers. These proportions are a semiquantitative measure of the relative abundance of the metal in different sites. To further constrain the abundance and distribution of metals, the XAS analysis was supplemented by elemental maps from EM and SIMS to correlate bulk molecular information with element distribution in and/or on sediment grains.

Experimental Section

Samples. Zinc- (1−2 wt %), cadmium- (50−300 ppm), and lead- (500−2000 ppm) bearing sediments were hand-collected from the bottoms of two drainages, Mineral Branch (MB) and Tar Creek (TC), in the U.S. Tri-State Mining District (Figure 1). Sediments were sieved and lightly hand-crushed with an agate mortar and pestle (see (ref 2) for details of sample collection). No significant differences were noted in the bulk chemistry among different sample size fractions. Results of bulk chemical analysis by ICP-AES and XRD are given in Table 1. Two precipitated zinc hydroxide samples were prepared according to procedures given by Christensen (*11*) (for $Zn(OH)_2$ − 1) and Dietrich and Johnson (*12*) (for $Zn(OH)_2$ − 2) and freeze-dried before data collection. A coprecipitated zinc−ferrihydrite sample (Zn−HFO) was prepared by methods described elsewhere (*13, 14*).

XAS Data Collection and Analyses. Absorption spectra for sediments were collected at the Stanford Synchrotron Radiation Laboratory (SSRL) on wiggler beamline 4-3 and bending magnet beamline 2-3 at cryogenic temperature (10−15 K) under dedicated conditions (3 GeV, 40−99 mA) using an unfocused beam. Powdered stream sediment samples were loaded into 1 mm thick Al or Teflon sample holders and sealed with Mylar film. For Zn XAS samples in which total iron concentration was high, samples were diluted 1:5 or 1:10 with $B(OH)_3$; all other XAS samples were undiluted. Zinc (9.4 to 10.7 keV; $k \approx 3$ to 12−15 Å^{-1}) and cadmium (26.5 to 27.8 keV; $k \approx 3$ to 13−17 Å^{-1}) K-edge XAFS spectra were

TABLE 1. Bulk Major and Trace Element Concentrations and Primary Mineralogy of Sediments Analyzed by XAS

sample	MB06	MB30	TC43	TC43	TC69	TC81	TC81	TC25	TC95	TC95
size	E	E	C	E	B	B	D	E	B	E
fraction (mm)	<0.14	<0.14	0.32−0.63	<0.14	0.63−1.0	0.63−1.0	0.14−0.32	<0.14	0.63−1.0	<0.14
site	3	2	1	1	1	5	5	9	10	10
pH	7.2	8.0	6.5	6.5	6.4	5.7	5.7	7.2	6.9	6.9
Major Elements (wt %)										
Al	1.52	3.59	0.60	1.32	0.94	0.63	0.63	0.90	4.60	5.29
Ca	3.95	3.14	2.43	0.95	1.05	1.66	0.81	4.26	1.60	2.64
Fe	2.41	6.28	11.64	32.51	14.01	64.97	65.92	0.76	2.91	3.85
K	0.40	0.94	0.21	0.23	0.10	0.04	0.06	0.25	0.73	0.75
Mg	0.11	0.25	0.84	0.35	0.48	0.10	0.11	1.28	0.73	1.20
Mn	0.03	0.17	0.02	0.03	0.03	0.01	0.10	0.02	0.12	0.21
Na	0.10	0.22	0.09	0.06	0.06	0.06	0.06	0.06	0.17	0.15
Si	35.14	31.38	26.56	20.66	26.26	1.35	1.39	33.62	26.64	31.25
Zn	1.03	2.06	6.14	1.97	8.53	1.76	1.73	2.47	2.42	2.89
Trace Elements (ppm)										
Ba	154	404	44	93	138	0	0	61	242	289
Cd	44	112	265	186	328	0	366	90	48	96
Cu	0	45	177	23	109	0	0	67	48	168
Pb	549	247	840	1625	1291	433	537	1771	145	433
Sr	44	90	44	23	22	24	24	45	48	72
Mineralogy (Major Phases by XRD)[a]										
	quartz calcite sphal	quartz calcite	quartz goeth calcite	quartz goeth	quartz goeth dolom	amorp	amorp	quartz calcite dolom	quartz	quartz dolom goeth

[a] sphal, sphalerite; goeth, goethite; dolom, dolomite; amorp, amorphous (mostly iron oxyhydroxide).

collected using a Si(220) monochromator crystal; lead L_{III}-edge spectra (13.1 to 14.7 keV; k ≈ 2.5 to 13−15 Å^{-1}) were collected using a Si(111) crystal. Fluorescence spectra were measured with either a 13-element solid-state Ge-array detector (for Zn, Cd, and Pb XAS) or a Stern-Heald-type detector (for Zn XAS) (*15*). Energy was calibrated by assigning the first inflection on the foil spectrum to an energy of 9659 eV for Zn, 13 035 eV for Pb, and 26 711 for Cd. Harmonic rejection was achieved by detuning the incoming beam by 30−50% of maximum intensity. Depending on absorber concentration and background noise, 3−32 scans were collected and averaged for each sample. Spectra for solid reference compounds (Table 2) were collected in order to calibrate fit parameters for theoretically calculated phase shift and amplitude functions and to estimate errors in fit results. Reference compounds were diluted with inert $B(OH)_3$ to produce ≈30% transmission of the incoming beam, and spectral data was collected using N_2-, Ar-, or Kr-filled ion chambers (depending on the absorber element).

Data analysis procedures are described in detail in O'Day et al. (*16*, *17*). Briefly, numerical results were extracted from the XAFS spectra using a curved-wave formalism and a single-scattering approximation (reviewed in refs 3, 18, and 19) implemented in the computer code EXAFSPAK (G. George, SSRL). Normalized, background-subtracted XAFS for reference and unknown spectra were filtered over similar *k* ranges ($k \approx 3$ to 12−17 Å^{-1}) and Fourier-transformed (square windowing) to produce radial structure functions (RSFs) that isolate frequency correlations between the central absorber atom and backscattering atoms as a function of distance (*R*). Fourier transforms shown here are uncorrected for phase shifts of the backscattering atoms. Nonlinear least-squares methods were used to fit unknown spectra to theoretical reference XAFS phase-shift and amplitude functions generated with the ab initio computer code FEFF6 (*20*−*22*) using atomic clusters from reference compounds as input. The theoretical FEFF functions were fit to experimental XAS data for the reference compounds in Table 2 to determine values for σ^2 and S_0^2, and to estimate fit errors. Typically for unknown spectra, distance (*R*), number of backscatterers (*N*), and a Debye−Waller term that accounts for thermal and static disorder (σ^2) were treated as adjustable parameters for each set of backscattering atoms at the same distance. The difference in threshold energy (ΔE_o) between theoretical reference functions and the unknown spectrum was treated as a single adjustable parameter for all sets of backscattering atoms for each sample (*17*). Reference functions were fit initially to filtered XAFS spectra of individual peaks in the RSFs to determine backscatterer identities and interatomic distances. Final fits were done on the full, normalized spectra to remove effects of finite window width in back transformation and to properly assess fitting errors.

Errors in fitted XAFS parameters were estimated by treating spectra of known reference compounds as unknowns and comparing the results with distance and coordination numbers obtained from published XRD data (Table 2). In general, XAFS fits of zinc and cadmium compounds agreed with XRD data to within $R \pm 0.02$ Å and $N \pm 30\%$ for first-coordination shells of O and S and second coordination shells of Zn, Fe, and Cd for chemically pure compounds. For lead, errors are more difficult to quantify owning to the irregularity of the Pb site in many compounds. For the crystalline compounds PbS and $PbCO_3$, fitted *R* values were within ±0.03 Å of XRD values for first and second shells. Fitted *N* values compared poorly with known coordination numbers (±40% or greater), probably because of static disorder and uncertainty in the value of S_0^2. As such, we place more weight on fitted *R* values than on fitted *N* values in the sediment XAFS spectra in our interpretations of metal coordination sites.

X-ray Diffraction (XRD), Electron Microprobe (EM), and Secondary Ion Mass Spectrometer (SIMS) Analysis. Powder XRD was used to determine the major mineralogy of the sediment samples (Table 1). All samples were scanned between 10° and 70° 2θ. Representative samples (3 high iron; 3 low iron) for which XAS spectra were collected were also examined by EM and SIMS. Powdered samples (<0.14 mm size fraction) were either sprinkled on sticky carbon tape or slurried in DI water, spread on 2 μm polycarbonate filter paper, and dried. The tape or filter paper was then mounted on Al disks and carbon coated. Electron microscopy was done on a JEOL Superprobe 866; SIMS analysis was done on Cameca IMS 3F. X-ray dots maps of particles were

TABLE 2. Reference Compounds for XAS Analyses[a]

mineral	formula	metal CN	first-shell coordination	ref
		Zinc Compounds		
franklinite	$ZnFe_2O_4$	4	4 O: 2.00 Å	36
hydrozincite	$Zn_5(OH)_6(CO_3)_2$	4,6	Oh[b](1): 4 OH: 2.10 Å 2 O: 2.12 Å Oh[b](2): 2 OH: 2.04, 2.10 Å 2 O: 2.16 Å Td[b](3): 1 OH: 1.98 Å 2 OH: 1.99 Å 1 O: 1.85 Å	37
sphalerite	ZnS	4	4 S: 2.34 Å	38
smithsonite	$ZnCO_3$	6	6 O: 2.11 Å	39
willemite	Zn_2SiO_4	4	1 O: 1.94, 1.95, 1.97, 1.98 Å	40
zinc hydroxide	γ-$Zn(OH)_2$	4	1 OH: 1.89, 1.94, 1.98, 2.03 Å	11
zinc hydroxide	ϵ-$Zn(OH)_2$	4	1 OH: 1.94, 1.95, 1.97, 1.98 Å	41
zincite	ZnO	4	2 O: 1.97, 1.99 Å	42
zincosite	$ZnSO_4$	6	2 O: 1.97, 2.11, 2.31 Å	43
		Cadmium Compounds		
cadmium sulfate	$CdSO_4$	4	2 O: 2.22 Å 1 O: 2.28, 2.42 Å	44
hawleyite	CdS	4	4 S: 2.52 Å	45
monteponite	CdO	6	6 O: 2.35 Å	46
otavite	$CdCO_3$	6	6 O: 2.29 Å	47
sphalerite	Cd/ZnS[c]	4	4 S: 2.48 Å	this study
		Lead Compounds		
galena	PbS	6	6 S: 2.97 Å	48
lead oxide	PbO (orthorhombic)	6	2 O: 2.22, 2.25, 2.48 Å	26
cerussite	$PbCO_3$	9	1 O: 2.62 Å 2 O: 2.66, 2.67 Å 2 O: 2.71, 2.77 Å	49
calcite	Pb/$CaCO_3$[d]	6	5 O: 2.53 Å	this study
hydrozincite	Pb/$Zn_5(OH)_6(CO_3)_2$[e]	?	1.5 O: 2.43 Å	this study

[a] Structures and interatomic distance from X-ray diffraction except for substituted compounds where interatomic distances and coordination numbers are from least-squares fits of experimental XAFS data. [b] Oh, octahdedral site; Td, tetrahedral site. [c] Natural sphalerite containing 1−2 wt % Cd substituting for Zn. [d] Natural calcite containing 1−2 wt % Pb substituting for Ca. [e] Natural hydrozincite containing 1−2 wt % Pb substituting for Zn.

generated with the EM and compared with scanning electron and secondary electron backscattered images. For minor elements not detectable with EM (Cd, Pb), element mass spectra were collected on the SIMS using either point mode analysis or by ion imaging using a fluorescent screen assemblage (*23*) and compared with major element distributions.

Results

Zinc. Figure 2a,b shows the XAFS and Fourier transforms of zinc in the mine sediments. Quantitative analysis of these spectra can easily distinguish first-shell coordination around zinc as ligation by sulfur atoms, oxygen atoms, or a mixture of both types of atoms. The interatomic distances and fitted number of sulfur backscatterers determined from quantitative analysis clearly indicate sulfur coordination indicative of a sulfide phase (Zn−S = 2.31−2.33 Å; N = 1.8−4.0). Likewise, most of the spectra exhibit backscattering from second-neighbor zinc atoms at distances of 3.80−3.85 Å and backscattering from another set of sulfur atoms at 4.46−4.50 Å (Table 3). These distances are consistent with those determined crystallographically for sphalerite (ZnS), the primary host ore for zinc in this area. In all of the samples but one, the XAS spectra show that sphalerite is clearly present as a detrital mineral in the sediments.

In addition to a distinct spectral signal from sphalerite, half of the sample spectra also indicate a fraction of zinc that is coordinated by oxygen atoms. At one sampling site (TC43), XAFS spectra were collected for two different size fractions: 0.23−0.63 mm (C) and <0.14 mm (E). The larger size fraction shows only a sphalerite component, whereas the smaller size fraction has about one-third sphalerite component and about two-thirds oxide component (Figure 3 and Table 3). For all samples with a Zn−O component, best fits of XAFS spectra give Zn−O distances of 1.98−2.00 Å, indicative of tetrahedral coordination of zinc by oxygen as the dominant mode of first-shell Zn−O coordination. At distances greater than first shell, subtraction of Zn−Zn backscattering in sphalerite (R = 3.80−3.85 Å) from the spectra clearly shows other components of second-neighbor backscattering (Figure 3). This backscattering can be attributed to either zinc or iron atoms. The fitted Zn−Zn/Fe distances are variable (3.08−3.52 Å), and in several samples, there are at least two sets of Zn−Zn/Fe backscatterers at different distances (Table 3). Owing to similarities in the phase-shift and amplitude backscattering functions of zinc and iron at the observed distances, neither zinc nor iron as the assumed atomic backscatterer produced a significantly better fit in most cases. Goodness-of-fit parameters (reduced χ^2) assuming either Zn or Fe atoms were within 1% when fitted with the same number of variables (see ref 17 for a discussion of fitting and error analysis). Thus, it is difficult to determine directly whether second-neighbor backscattering is from Fe, Zn, or a mixture of both Fe and Zn atoms.

The Zn-XAFS spectra clearly indicate the presence of a sulfide phase, but the nature of the oxide phase associated with zinc is less obvious. A variety of possible phases were tested based on the observed Zn−O distances. The fitted Zn−O distances of 1.98−2.00 Å indicate primarily 4-fold coordination for zinc, ruling out coordination in carbonate or sulfate phases, which are strictly 6-fold (R_{Zn-O} > 2.1 Å). Likewise, the spectrum for zinc in hydrozincite ($Zn_5(OH)_6(CO_3)_2$), a common metastable phase in which zinc is both

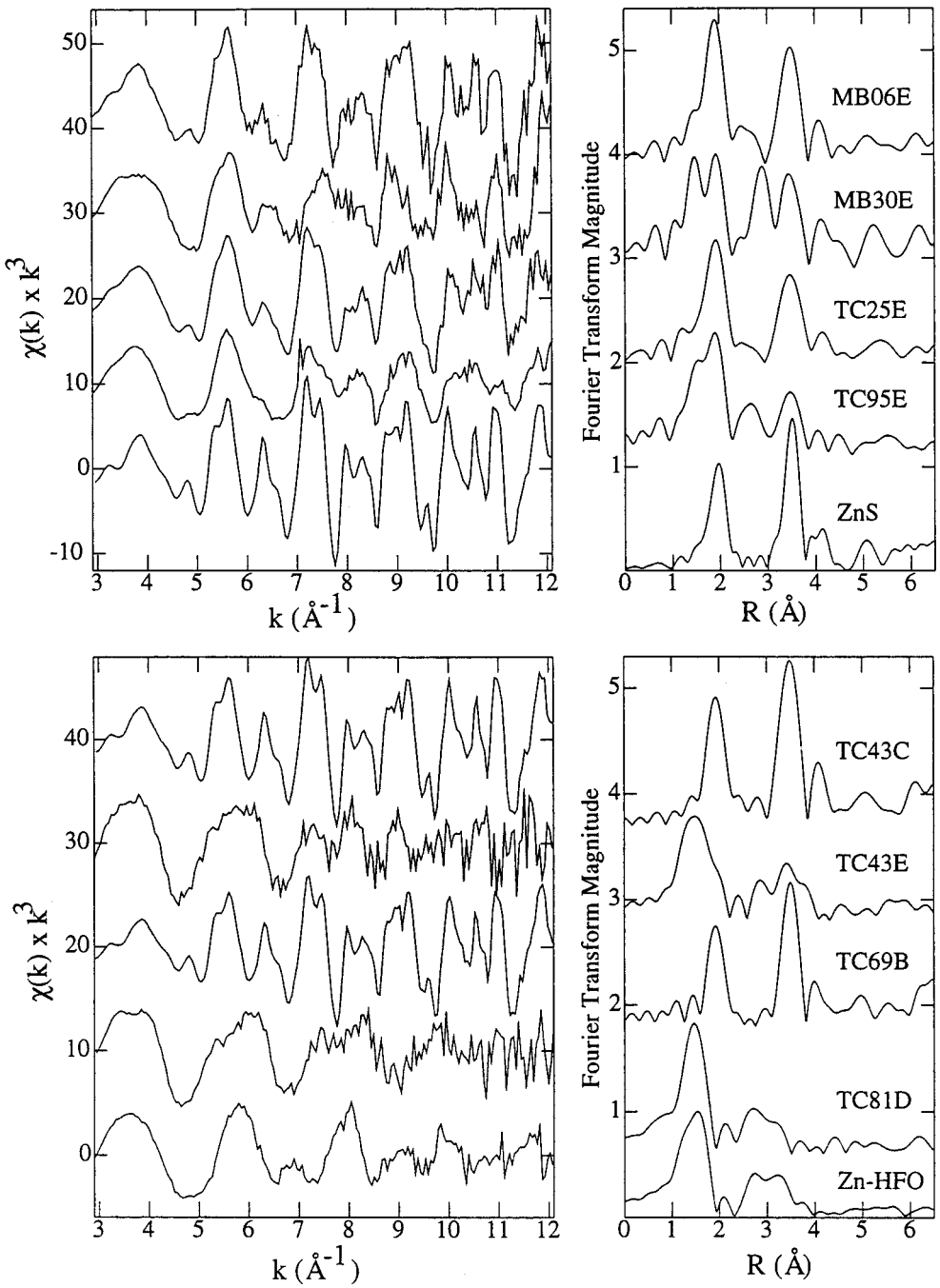

FIGURE 2. Normalized Zn-XAFS spectra (left) weighted by k^3 and Fourier transforms (right) of stream sediments from the Mineral Branch (MB) and Tar Creek (TC) drainages shown in Figure 1. In the top panels, spectra of sediments with low total Fe contents are compared with that of crystalline sphalerite (ZnS, bottom spectrum). In the bottom panels, spectra of sediments with high total Fe are compared with a laboratory sample of Zn coprecipitated with ferrihydrite (Zn−HFO, bottom spectrum).

4- and 6-fold coordinated by oxygen, does not match the spectra of the sediment samples. There is no evidence in the spectra for backscattering from silicon or aluminum, which might indicate either coordination in hydrous Al- or Si-bearing phases or adsorption onto the surfaces of quartz or aluminosilicate minerals. In two samples in which the bulk iron concentration is high (TC43E, TC81D), it is likely that amorphous iron oxyhydroxides are the primary host phase for zinc after it is removed from sphalerite. In the high-iron samples, fitted N and σ^2 values for first-shell oxygen atoms are higher than in low-iron samples (MB30E, TC95E; Table 3). Because these two parameters are highly correlated in fitting, interpretation of their absolute values is suspect. The overall increase in N and σ^2, however, is evidence for a difference in average zinc coordination, perhaps indicating increased disorder, between high- and low-iron samples. The XAFS spectra of high-iron samples were fit slightly better assuming only Fe atoms as second-neighbor backscatterers (about 2%); fits with only second-neighbor Zn atoms were not robust (i.e., some parameters converged to unrealistic values). In the low-iron samples, fits assuming only zinc or only iron did not differ significantly. We also note that, overall, second-neighbor zinc or iron coordination numbers are low ($N \leq 2$), suggesting the absence of a well-ordered precipitate.

For comparison to the sediment samples, we analyzed the Zn-XAFS spectra of two experimentally precipitated zinc hydroxides and one coprecipitated zinc−iron oxyhydroxide

TABLE 3. Quantitative Analyses of Zn XAFS Spectra

	Sediment Samples												
	sphalerite component						oxide component						
	Zn−S			Zn−Zn			Zn−O			Zn−Zn/Fe[a]			
	R (Å)	*N*	σ^2 (Å^2)	*R* (Å)	*N*	σ^2 (Å^2)	*R* (Å)	*N*	σ^2 (Å^2)	*R* (Å)	*N*	σ^2 (Å^2)	ΔE_0 (eV)[b]
MB06E	2.32	3.7	0.0047	3.82	4.2	0.0028							−6.8
	4.48	6.8	0.0059										
MB30E	2.32	1.6	0.0026	3.81	5.5	0.0099	1.97	2.2	0.0039	3.22	2.0	0.0022	−8.3
TC25E	2.33	3.2	0.0043	3.83	6.6	0.0071							−5.5
	4.50	4.5	0.0060										
TC43C	2.33	3.1	0.0015	3.83	9.4	0.0036							−7.0
	4.48	9.0	0.0033										
TC43E[c]	2.33	0.8	0.0043	3.85	1.6	0.0047	2.00	3.2	0.0072	3.36	0.8	0.0021	−2.0
										3.52	1.6	0.0053	
TC69B	2.33	4.0	0.0041	3.83	8.3	0.0033							−7.4
	4.49	7.5	0.0042										
TC81D[c]							1.98	5.7	0.0095	3.30	1.3	0.0021	−10.2
										3.46	1.5	0.0028	
TC95E	2.32	2.0	0.0038	3.80	2.4	0.0051	2.00	2.3	0.0064	3.07	0.9	0.0031	−8.7
										3.17	0.7	0.0066	

	Precipitated Compounds									
	Zn−O			Zn−Zn			Zn−Fe			
	R (Å)	*N*	σ^2 (Å^2)	*R* (Å)	*N*	σ^2 (Å^2)	*R* (Å)	*N*	σ^2 (Å^2)	ΔE_0 (eV)[b]
$Zn(OH)_2$ − 1	1.95	3.6	0.0097	3.14	3.1	0.0044				−3.8
	2.08	3.8	0.0060	3.57	4.1	0.0042				
$Zn(OH)_2$ − 2	1.92	1.9	0.0082	3.08	2.3	0.0035				−3.7
	2.04	4.4	0.0044	3.56	2.0	0.0035				
Zn−HFO	1.92	(2.0)[d]	0.0047	3.54	1.2	0.0042	3.12	0.7	0.0035	−6.6
	2.04	(2.0)[d]	0.0033							

[a] Second-neighbor backscatterers are Zn or Fe. [b] Difference in $k = 0$ energy between unknown spectrum and theoretical reference functions calculated by FEFF6. [c] Second-shell backscatterers in the oxide component are probably Fe. [d] Parameter fixed during least-squares fit.

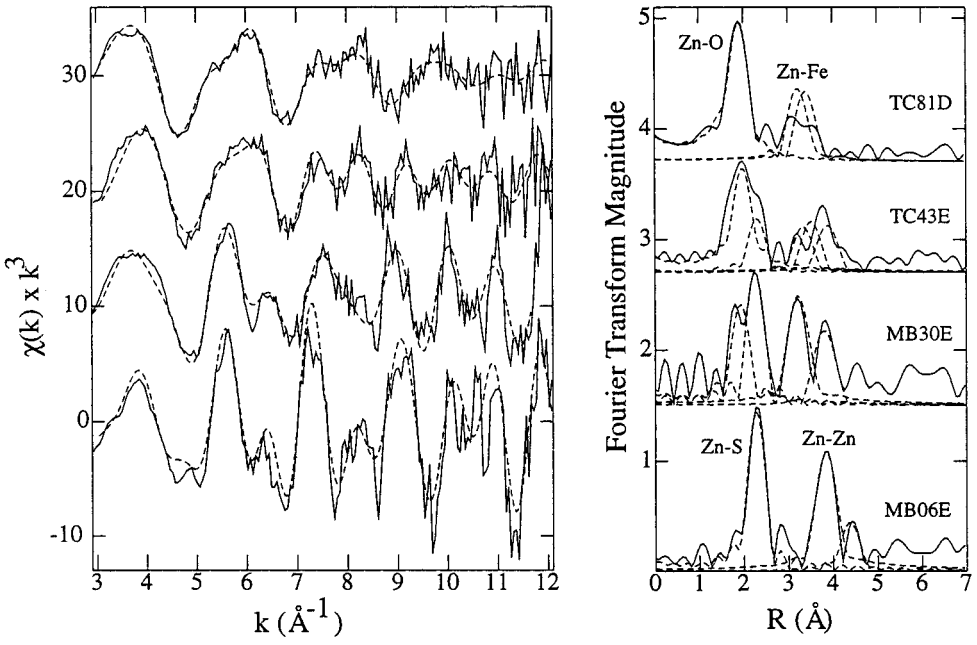

FIGURE 3. Least-squares fits (left, dashed lines) of selected Zn-XAFS spectra (solid lines) and Fourier transforms (right) from Figure 2. In the Fourier transforms, fits (dashed lines) are deconvolved into individual backscattering components.

(Table 3). Interatomic distances derived from least-squares fits of the zinc hydroxides do not match distances from structure determinations by XRD for γ-$Zn(OH)_2$ and ϵ-$Zn(OH)_2$ (Table 2). The XAFS spectra are fit with two first-shell Zn−O distances and two second-shell Zn−Zn distances that are not consistent with those derived from XRD (*11, 12*). For the coprecipitated zinc−iron oxyhydroxide (Zn−HFO), best fits of the spectrum suggest a mixture of zinc and iron second-neighbor backscatterers. In general, second-neighbor Zn−Zn/Fe distances are not diagnostic of a particular phase for either the sediment samples or the experimental precipitates.

It is unlikely that the XAFS spectra of the sediment samples represent a compound in which zinc is bonded to both oxygen and sulfur atoms. The spectral analysis clearly indicates first and higher shell backscattering from atoms in sphalerite at expected crystallographic distances. If zinc was removed

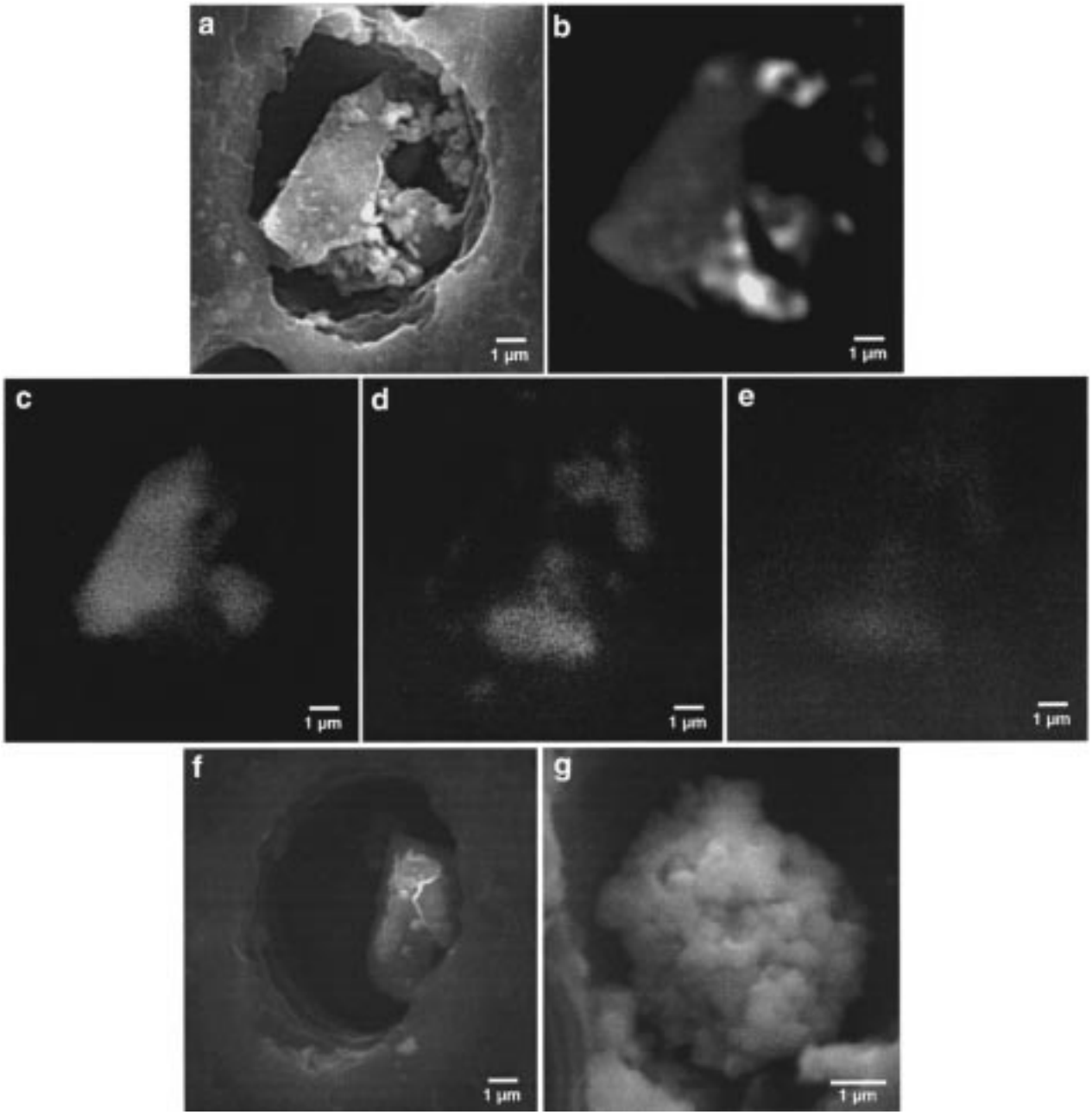

FIGURE 4. Secondary (SE) and backscattered electron (BE) images and X-ray elemental dot maps for particles from sample TC43E (particles are trapped in 2 μm filter pores): (a) SE image of a quartz grain with Fe surface particles; (b) BE image of the same particle; (c−e) X-ray elemental dot maps for Si, Fe, and Zn, respectively, of particle a. Note the correlation of Fe and Zn with some of the bright portions of the BE image. This may be residual sphalerite; (f) sphalerite (ZnS) grain with Fe surface particles; (g) iron oxyhydroxide particle.

from sphalerite and coordinated in a single phase by both oxygen and sulfur ligands, the average number of sulfur ligands would be much less than four and the Zn−S interatomic distance would change significantly. We interpret these spectra as a physical mixture of different sulfide and oxide phases, and this interpretation is corroborated by EM and SIMS particle analysis. Examination of the sediments with SEM, electron-backscatter imaging, and EDS analysis shows, in high-iron samples, the predominance of iron in a surface phase on detrital particles, mostly quartz. Spot analyses and element maps for silicon, iron, and zinc indicate an association of zinc and iron (Figure 4). The sulfur X-ray signal (not shown) was weak but correlated roughly with zinc. Large, unaltered sphalerite particles are scarce. Residual sphalerite particles appear to be less than 1 μm in size and to have iron on the surface (Figure 4). The close association of residual sphalerite and iron-bearing-phase surface coatings suggest removal of zinc from sphalerite and its incorporation into iron oxyhydroxides on mineral surfaces.

Cadmium. Cadmium is found in the Tri-State District as a substituent for zinc in sphalerite. Fits of XAFS spectra of pure CdS (isomorphic with sphalerite) and cadmium in natural sphalerite (0.5 wt % Cd) produces Cd−S and Cd−Cd interatomic distances slightly longer than Zn−S and Zn−Zn distances in pure ZnS because of the larger cation size of Cd^{2+} (Tables 3 and 4; Figure 5). From least-squares fits of cadmium XAFS for the reference sphalerite, the ratio of Zn:Cd is about 10:2, compared with 12 Zn or 12 Cd atoms in pure ZnS or CdS, respectively (Table 4). If cadmium were randomly distributed in sphalerite, a lower Zn:Cd ratio is expected in the XAFS spectrum. This suggests clustering or domains of CdS in the sphalerite that are consistent with mineralogical observations of sulfide ores (*24*).

TABLE 4. Quantitative Analyses of Cd XAFS Spectra

	Sediment Samples									
	Cd−S			Cd−Zn			Cd−Cd			
	R (Å)	*N*	σ^2 (Å^2)	*R* (Å)	*N*	σ^2 (Å^2)	*R* (Å)	*N*	σ^2 (Å^2)	ΔE_0 (eV)[a]
TC43C	2.50	3.9	0.0021	3.89	11.8	0.0040	4.19	2.3	0.0042	−8.9
	4.50	7.0	0.0049	5.44	5.6	0.0040				
TC69B	2.49	3.9	0.0023	3.87	9.9	0.0035	4.19	3.4	0.0033	−8.7
	4.53	10.7	0.0031	5.43	5.5	0.0036				
TC95B	2.51	3.2	0.0027	3.89	2.3	0.0070				−9.9
TC95E	2.51	4.1	0.0025							−6.5

	Cd−S			Cd−Zn			Cd−Ca			
	R (Å)	*N*	σ^2 (Å^2)	*R* (Å)	*N*	σ^2 (Å^2)	*R* (Å)	*N*	σ^2 (Å^2)	ΔE_0 (eV)[a]
TC25E	2.52	3.5	0.0011	3.88	7.9	0.0059	4.07	5.0	0.0056	−6.4
	4.51	4.9	0.0027							
	Cd−O									
	2.27	3.1	0.0032							

	Reference Compounds									
	Cd−S			Cd−Zn			Cd−Cd			
	R (Å)	*N*	σ^2 (Å^2)	*R* (Å)	*N*	σ^2 (Å^2)	*R* (Å)	*N*	σ^2 (Å^2)	ΔE_0 (eV)[a]
Cd/ZnS[b]	2.51	(4.0)[c]	0.0013	3.89	11.8	0.0040	4.17	(2.0)[c]	0.0038	−8.5
	4.51	(12.0)[c]	0.0049	5.44	5.6	0.0040				
CdS	2.51	(4.0)[c]	0.0013				4.12	(12.0)[c]	0.0037	−8.7
	4.81	(12.0)[c]	0.0096				5.83	(6.0)[c]	0.0037	

[a] Difference in $k = 0$ energy between unknown spectrum and theoretical reference functions calculated by FEFF6. [b] Natural sphalerite (ZnS) sample with ppm levels of Cd substituting for Zn. [c] Parameter fixed during least-squares fit.

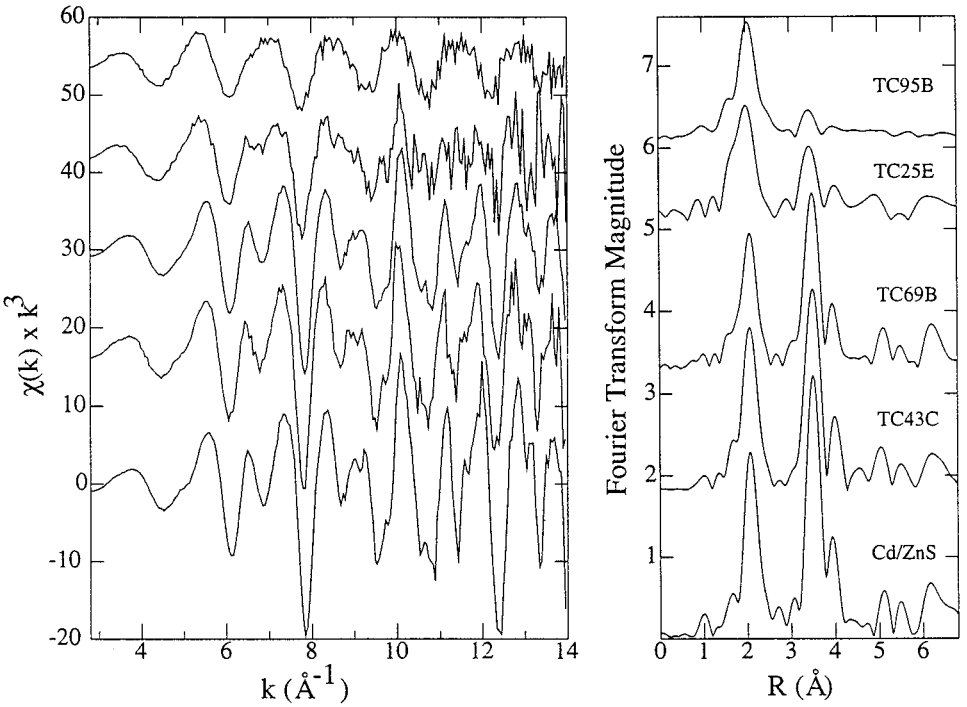

FIGURE 5. Normalized Cd-XAFS spectra (left) weighted by k^3 and Fourier transforms (right) of stream sediments from the Tar Creek (TC) drainage shown in Figure 1. The bottom Cd spectrum (Cd/ZnS) is a sample of sphalerite ore from the area containing 0.5 wt. % Cd substituting for Zn.

We collected Cd-XAFS spectra for only half of the stream sediments samples for which zinc was measured because of much lower cadmium concentrations (0−300 ppm) and because of high background fluorescence in samples with high bulk iron concentrations. In all of the samples studied, analysis of the Cd-XAFS indicates that cadmium is bonded by sulfur atoms at distances indicative of sulfide (Figure 6). Interatomic Cd−S and Cd−Cd distances are identical with those obtained from the reference sphalerite sample (Table 4), and there is no evidence for coordination of cadmium by oxygen in any of the samples, except for one sample (TC25E). In this sample, first-shell backscattering is dominated by sulfur atoms, but there is a secondary signal from oxygen scatterers at a distance indicative of bonding in a carbonate

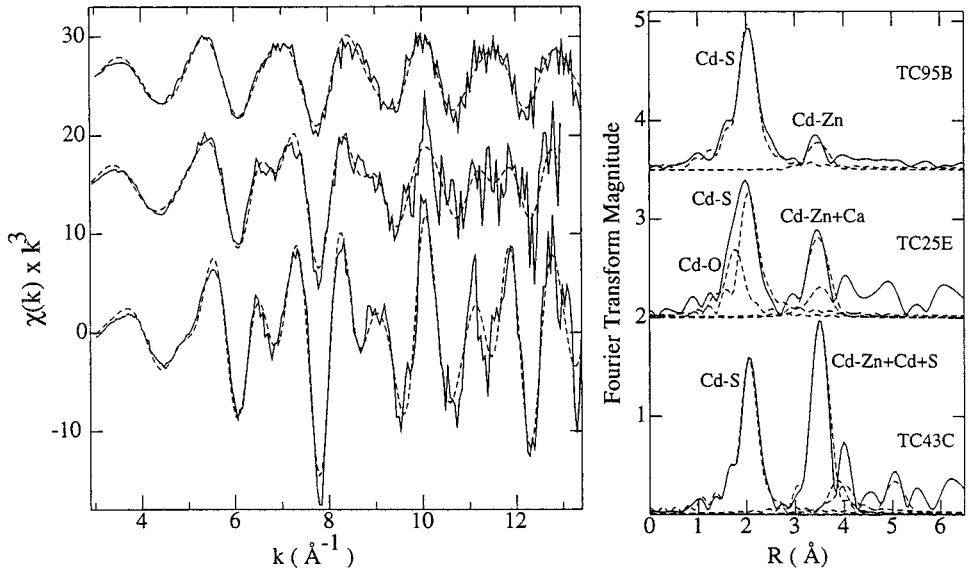

FIGURE 6. Least-squares fits (left, dashed lines) of selected Cd-XAFS spectra (solid lines) and Fourier transforms (right) from Figure 5. In the Fourier transforms, fits (dashed lines) are deconvolved into individual backscattering components. Note in the spectrum of TC25E, the presence of Cd−O first-shell and Cd−Ca second-shell backscatterers indicative of Cd substitution in calcite ($CaCO_3$).

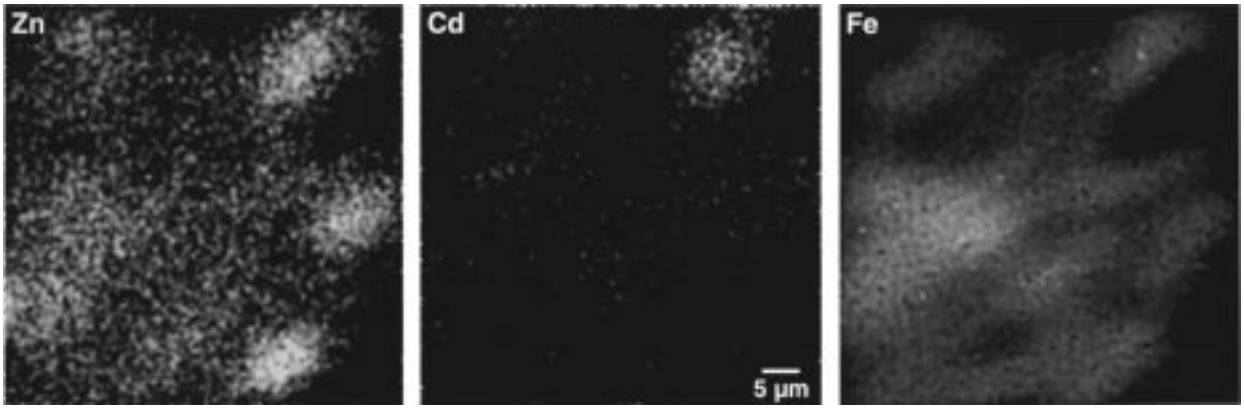

FIGURE 7. SIMS fluorescent screen imaging of sample TC81D for Zn, Cd, and Fe. Particles are generally <2 μm, and Fe coatings are ubiquitous on grains. The bright Cd patch in the upper right corner that correlates positively with Zn is probably small residual sphalerite particles. Total Fe in the sample is 65 wt %.

phase, probably calcite (Figure 6). Results from least-squares fits suggest that cadmium in TC25E is distributed between sphalerite and calcite in a ratio of about 4:1. In sample TC95E, cadmium is four-coordinated by sulfur atoms at 2.51 Å (indicative of sphalerite), but the number of second-neighbor zinc atoms (at 3.89 Å) around cadmium is significantly reduced (from 12 to ≈2; Figure 6). This result may indicate that crystalline sphalerite particles in the sediments are weathering and becoming disordered or increasing in atomic vacancies, perhaps because of clustering of cadmium in sphalerite, giving rise to the low intensity of second-neighbor backscattering. In this sample, the Zn-XAFS spectra indicate zinc bonding in both sphalerite and an oxide phase, but cadmium is clearly not being incorporated into a secondary oxide phase as is zinc.

Results of element mapping of particles in four samples with SIMS gave a weak cadmium signal that was mostly correlated with zinc. Because particle size (<2−10 μm) was smaller than the ion spot size (≈20 μm), it was difficult to resolve the cadmium spatial distribution in individual particles. Fluorescence screen imaging, however, was useful for showing positive or negative element correlations for particles spread over larger areas (≈50 × 50 μm). In a high-iron sample (TC81D), no evidence was found for significant association of cadmium with iron (Figure 7). In low-iron samples, cadmium was associated with zinc and sulfur, consistent with the Cd-XAFS data indicating cadmium substitution in sphalerite.

Lead. In the same sediment samples studied by zinc and cadmium XAS, we attempted to collect absorption spectra for lead. Although total lead concentrations are higher than cadmium concentrations in all of the samples, it was difficult to obtain good signal-to-noise for lead XAFS. This is because of (i) the lower energy of the Pb-absorption edge (13 035 eV) as compared to the Cd-edge (26 711 eV), (ii) weaker fluorescence for a L_{III}-absorption edge (Pb) as compared to a K-absorption edge (Cd), and (iii) higher static disorder for Pb atomic sites in mineral phases than for Cd atomic sites. Qualitatively, the Pb-XAFS spectra are not indicative of lead coordination in a sulfide phase (Figure 8). In three samples for which usable XAFS data was obtained, analysis of the first coordination shell indicates lead bonding by oxygen at distances consistent with carbonate and/or oxide phases (Table 5). There is no evidence for coordination by sulfur, which would be quite apparent from the shape of the main absorption edge. In sample TC25E, for which data was obtained to $k = 13$ Å^{-1}, the first-shell Pb−O distance (2.65 Å) is in the range expected for lead carbonate phases (≈2.5−2.7 Å). In this sample, high amplitude oscillations at high k result from Pb−Pb second-neighbor backscattering at

TABLE 5. Quantitative Analyses of Pb XAFS Spectra

	Sediment Samples						
	Pb−O			Pb−Pb			
	R (Å)	N	σ^2 (Å^2)	R (Å)	N	σ^2 (Å^2)	ΔE_0 (eV)[a]
TC25E	2.65	0.6	0.0010	4.22	1.4	0.0029	−6.1
				5.00	1.3	0.0036	
TC43E	2.32	3.9	0.0060				−10.0
	2.56	3.1	0.0066				
	3.35	5.0	0.0097				
TC95B	2.39	2.3	0.0090				−10.0
	2.59	2.3	0.0063				
	3.31	2.0	0.0058				

	Reference Compounds									
	Pb−O			Pb−C			Pb−Pb			
	R (Å)	N	σ^2 (Å^2)	R (Å)	N	σ^2 (Å^2)	R (Å)	N	σ^2 (Å^2)	ΔE_0 (eV)[a]
$PbCO_3$	2.66	(9.0)[b]	0.0092	3.08	3.0	0.0039	4.19	(2.0)[b]	0.0025	0.5
							4.97	(4.0)[b]	0.0025	
							5.19	(2.0)[b]	0.0059	

	Pb−O			Pb−Ca			
	R (Å)	N	σ^2 (Å^2)	R (Å)	N	σ^2 (Å^2)	ΔE_0 (eV)[a]
$Pb/CaCO_3$[c]	2.53	4.8	0.0037	4.11	7.5	0.0045	−7.0

[a] Difference in $k = 0$ energy between unknown spectrum and theoretical reference functions calculated by FEFF6. [b] Parameter fixed during least-squares fit. [c] Natural calcite ($CaCO_3$) sample with ppm levels of Pb substituting for Ca.

distances similar to those of lead in cerussite ($PbCO_3$) (Figure 8b). In the other two samples, TC95E (2.9 wt % Fe) and TC43E (32.5 wt % Fe), the XAFS spectra can be fit with three Pb−O distances, although the uncertainty in this analysis is high due to the poor data quality and limited k range. The shorter Pb−O distances (2.32 and 2.39 Å) may indicate lead coordination in oxide or hydroxide phases, although Pb−O distances in these phases from XRD (*25*, *26*) and from XAFS studies of lead sorbed to aluminum and iron oxides (*27*, *28*) show significant static disorder in lead bonding. As a result, analysis of first-shell Pb−O bonding only (i.e., small k range) is not particularly diagnostic of lead phases. Although our data set is limited, it appears that incorporation of lead into carbonate phases, either as a substituent into calcite or formation of a lead carbonate phase, is one identifiable mode of lead uptake in the low-iron sediments we studied. In high-iron samples, it is possible that lead is associated with iron oxyhydroxides, as might be expected based on macroscopic studies of lead sorption on iron oxyhydroxide phases that show sorption occurring at relatively low pH (≈4−7 (*29*, *30*)).

Discussion

The microscopic information from XAS can be interpreted in terms of sediment chemistry and mineralogy to identify how metals are sequestered in solid phases in these contaminated streams. Sediment analyses by XRD (Table 1) indicate that the primary crystalline phases are quartz (α-SiO_2), calcite ($CaCO_3$), dolomite ($CaMg(CO_3)_2$), goethite (α-FeOOH), and in one sample, a minor amount of sphalerite (ZnS). X-ray amorphous samples with high bulk iron concentrations contain a large percentage of amorphous iron oxyhydroxide. Analyses of the XAFS spectra of the sediments highlight the persistence of sphalerite as a carrier of zinc and cadmium, even in sediments in which sphalerite was not identified by XRD. In addition to sphalerite, half of the samples examined had a Zn−O secondary phase. In these samples, fitting of the XAFS spectra indicated primarily tetrahedral coordination of zinc by oxygen and a low number (≈1−2) of either zinc or iron second-neighbor backscatterers. Silicate or aluminosilicate phases as the primary Zn−O component were ruled out based on comparisons with spectra of known compounds (Table 2) and on least-squares fits in which different atomic backscatterers were tested.

Although the exact phase of the Zn−O component in the sediments is not apparent from the XAFS analysis, we can interpret the local zinc atomic environment from the fitted interatomic distances and from comparison with precipitated zinc samples. Quantitative analysis of the XAFS spectra of two precipitated zinc hydroxide samples produced interatomic first- and second-neighbor distances that are not consistent with distances reported from XRD for these forms (γ-$Zn(OH)_2$ (*10*) and ϵ-$Zn(OH)_2$ (*12*)) in which zinc should only be tetrahedrally coordinated by oxygen. In our XAFS analysis of the precipitates, first- and second-neighbor interatomic distances indicate a mixture of tetrahedral and octahedral zinc (Table 3), suggesting that the precipitated forms were not aged to their stable structures before drying. In the low-iron sediment samples (MB30E, TC95E), relatively short second-neighbor Zn−Zn/Fe distances (3.07−3.22 Å), similar to the shorter Zn−Zn distance found in the precipitated samples (3.08 and 3.14 Å), may indicate the presence of some octahedrally coordinated zinc. In the high-iron samples (TC43E, TC81D), second-neighbor Zn−Zn/Fe distances are variable (3.30−3.52 Å) and could indicate either corner-sharing of Zn−Zn tetrahedra and/or corner-sharing of zinc tetrahedra and iron octahedra (Fe^{3+} is only octahedral). Examination by XAS of a series of experimentally precipitated and sorbed mixtures of zinc and amorphous iron oxyhydroxide by Waychunas et al. (*31*) indicates that zinc tetrahedra form bidentate, corner-sharing bonds to Fe−OH octahedra. Their study also suggests that zinc does not form an extensive solid solution with iron at high Zn:Fe ratios, but rather that zinc tetrahedra and iron octahedra tend to cluster locally. Their results together with the observations of this study suggest bidentate bonding of tetrahedral zinc to amorphous iron oxyhydroxide at relatively low Zn:Fe ratios. With increasing Zn:Fe, zinc may cluster locally in either tetrahedral

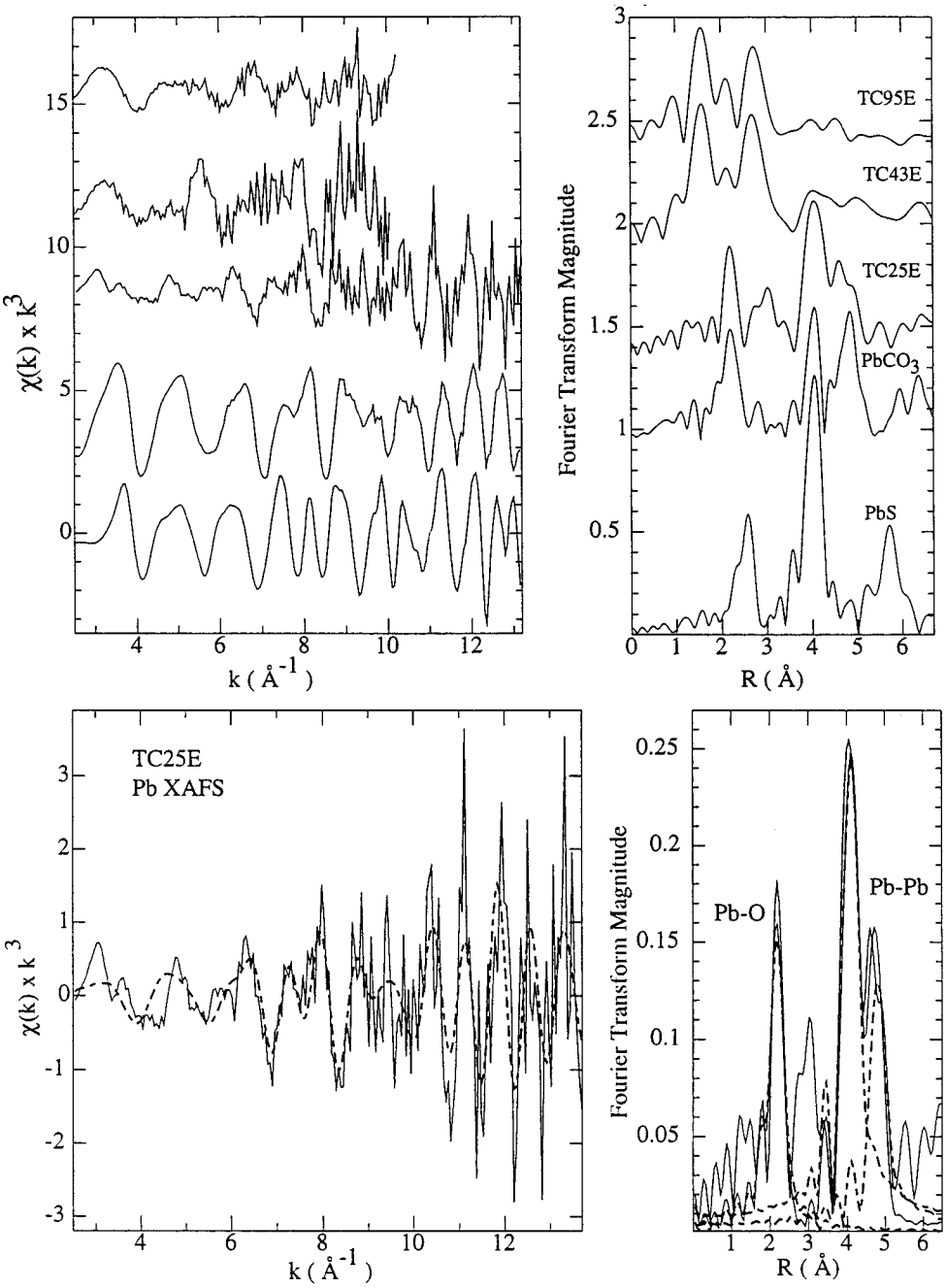

FIGURE 8. (a) Normalized Pb-XAFS spectra (left) weighted by k^3 and Fourier transforms (right) of stream sediments from the Tar Creek (TC) drainage shown in Figure 1 compared with two Pb reference compounds, cerussite ($PbCO_3$) and galena (PbS). (b) Least-squares fit (left, dashed line) of Pb XAFS of sample TC25E and its Fourier transform (right) assuming one shell of first-neighbor O atoms and two shells of second-neighbor Pb atoms (see Table 5). Dashed lines in the Fourier transform show the fit deconvolution into individual scattering components.

or octahedral coordination, perhaps as a disordered or amorphous precipitate. This analysis points out the variability and uncertainty in the structure of amorphous Zn−Fe oxyhydroxide phases, which relates directly to solubility measurements, and the difficulty in distinguishing sorption complexes from precipitates.

The behavior of cadmium in these samples is quite different from zinc even though both elements originate from the same ore mineral. There is no evidence that cadmium is being taken up by an oxyhydroxide phase, even in samples in which ≈50−75% of the zinc is bound in an oxyhydroxide phase (TC43, TC95). This observation raises the possibility that cadmium partitions preferentially into the aqueous phase under these solution conditions. The only evidence for cadmium incorporation into a secondary phase is in one sample (TC25E) in which a fraction of cadmium (≈25%) is apparently substituted into a carbonate phase, probably calcite. In one other sample, a large reduction in second-neighbor Zn atoms is evidence for the disintegration of the long-range sphalerite structure around cadmium, leaving residual Cd−S clusters in a disordered solid. Elemental imaging with SIMS indicates no association of cadmium with iron. Unlike zinc, XAFS analysis of laboratory samples has shown that cadmium retains its octahedral coordination upon sorption onto iron oxide minerals and ferrihydrite (*32*). Therefore, if cadmium was taken up by iron phases in the sediments in excess of ≈10% of total cadmium, this would be easily distinguished by XAFS because of the significant

spectral differences between sulfur and oxygen ligands. Both the XAFS and SIMS data are consistent with experimental sorption data showing little uptake of cadmium onto amorphous $Fe(OH)_3$ below pH ≈ 6.0 for low total cadmium concentrations (*33*). At the sample localities of this study, stream pH is generally about 6−7 at the nonacid sites, so significant adsorption of cadmium onto iron oxyhydroxides is not expected (see companion paper (ref 2), for detailed discussion).

For lead, there is no spectroscopic evidence for lead bonding in a sulfide phase. Apparently the host ore, galena (PbS), is less persistent in this system than sphalerite. Association of lead with a carbonate phase is suggested by a limited amount of XAFS data for low-iron samples. This is consistent with experimental studies of galena dissolution in the presence of air in which XPS results suggest the formation of a lead carbonate or lead hydroxycarbonate surface phase as galena dissolves (*34*). When significant amounts of iron oxyhydroxides are present, sorption of lead might be expected at low pH (<7), whereas competition between sorption onto iron oxyhydroxides and precipitation of carbonate phases may occur at higher pH (>7) depending on the amount of iron in the system.

The XAFS data provides a detailed, molecular level view of the different partitioning behavior of three divalent metals in a stream system. This kind of information, which is needed to constrain predictive models regarding metal sorption/desorption and long-term fate, cannot be derived from bulk measurements at these metal concentrations. In our XAS analysis, we have examined metal uptake in solid phases (rather than sorption on surfaces) by analyzing bulk, size-fractionated samples that have been air-dried. If metals were associated with solid phases via a surface complexation mechanism requiring a significant amount of bulk water (i.e., outer-sphere or diffuse-layer adsorption), this may have been altered by drying. The XAS samples were not chemically separated or treated before analysis, so alteration of the metal environment by extraction techniques has been avoided. The results of our analyses indicate that, for all three metals, uptake in or on secondary phases is apparently governed by the local pH and by the total amount of iron in the system, both of which determine whether an iron oxyhydroxide or a carbonate phase is the dominant metal carrier. There is no evidence that any other major phases are significant for metal uptake. From a quantitative modeling viewpoint, these observations greatly simplify the scope of chemical reactions that need to be considered in a geochemical or hydrogeochemical model. In our companion paper (*2*), we interpret the results of this spectroscopic study in the context of the chemistry of streamwaters at the sample sites, thermodynamic predictions of mineral saturation state, and dissolution rates of metastable ore minerals.

Acknowledgments

P.A.O. acknowledges financial support from the Arizona State University Faculty Grant-In-Aid Program and the National Science Foundation (EAR-9629276). Financial support was provided by the Institute of Geophysics and Planetary Physics (IGPP) and by the Laboratory Directed Research and Development Program under the auspices of Department of Energy Contract W-9405-ENG-48. SSRL is operated by the Department of Energy, Office of Basic Energy Sciences under Contract DE-AC03-76SF00515. Chris Fuller (USGS) provided the precipitated laboratory samples used in this study. We thank Jim Clark for EM analyses, Rick Hervig for SIMS analyses, Margaret Ebert and Matt Newville for assistance with XAS data collection, and Lara Heister and Mary Etsitty for assistance with EM and SIMS data collection.

Literature Cited

(1) Brown, G. E., Jr.; Parks, G. A.; O'Day, P. A. In *Sorption at mineral/water interfaces: Macroscopic and microscopic perspectives*; Vaughan, D. J., Pattrick, R. A. D., Eds.; Mineral Surfaces, Mineralogy Society Series 5; Chapman and Hall: London, 1995; pp 129−183.
(2) Carroll, S. A.; O'Day, P. A.; Piechowski, M. *Environ. Sci. Technol.* **1998**, *32*, 956−965.
(3) Brown, G. E., Jr.; Calas, G.; Waychunas; G. A. Petiau, J. In *X-ray absorption spectroscopy and its applications in mineralogy and geochemistry*; Hawthorne, F. C., Ed.; Spectroscopic Methods in Mineralogy and Geology, Review of Mineralogy 18; Mineralogical Society of America: Washington, DC, 1988; pp 431−512.
(4) Brown, G. E., Jr.; Parks, G. A.; Chisholm-Brause, C. J. *Chimia* **1989**, 43, 248−256.
(5) Charlet, L.; Manceau, A. In *Environmental Particles*; Buffle, J., Van Leeuwen, H. P., Eds.; Lewis Publishers: Chelsea, MI, 1993; pp 117−164.
(6) O'Day, P. A.; Carroll, S. A.; Waychunas, G. A.; Phillips, B. *Physica B* **1995**, *208/209*, 309−310.
(7) Manceau, A.; Boisset, M.-C.; Sarret, G.; Hazemann, J.-L.; Mench, M.; Cambier, P.; Prost, R. *Environ. Sci. Technol.* **1996**, *30*, 1540−1552.
(8) Morris, D. E.; Allen, P. G.; Berg, J. M.; Chisholm-Brause, C. J.; Conradson, S. D.; Donohoe, R. J.; Hess, N. J.; Musgrave, J. A.; Tait, C. D. *Environ. Sci. Technol.* **1996**, *30*, 2322−2331.
(9) Peterson, M. L.; Brown, G. E., Jr.; Parks, G. A., Stein, C. L. *Geochim. Cosmochim. Acta* **1997**, 61, 3399−3412.
(10) Crozier, E. D.; Rehr, J. J.; Ingalls, R. In *X-ray Absorption: Principles, Applications, Techniques of EXAFS, SEXAFS, and XANES*; Koningsberger, D. C., Prins, R., Eds.; Chemical Analysis 92; Wiley: New York, 1988; pp 373−442.
(11) Christensen, A. N. *Acta Chem. Scand.* **1969**, *23*, 2016−2020.
(12) Dietrich, H. G.; Johnston, J. *J. Am. Chem. Soc.* **1927**, *49*, 1419−1431.
(13) Waychunas, G. A.; Rea, B. A.; Fuller, C. C.; Davis, J. A. *Geochim. Cosmochim. Acta* **1993**, *57*, 2251−2269.
(14) Fuller, C. C.; Davis, J. A.; Waychunas, G. A. *Geochim. Cosmochim. Acta* **1993**, *57*, 2271−2282.
(15) Lytle, F. W.; Sandstrom, D. R.; Marques, E. C.; Wong, J.; Spiro, C. L.; Huffman, G. P.; Huggins, F. E. *Nucl. Instrum. and Methods* **1984**, *226*, 542−548.
(16) O'Day, P. A.; Brown, G. E., Jr.; Parks, G. A. *J. Colloid Interface Sci.* **1994**, *165*, 269−289.
(17) O'Day, P. A.; Rehr, J. J.; Zabinsky, S. I.; Brown, G. E., Jr. *J. Am. Chem. Soc.* **1994**, *116*, 2938−2949.
(18) Stern, E. A. In *X-ray Absorption: Principles, Applications, Techniques of EXAFS, SEXAFS, and XANES*; Koningsberger, D. C., Prins, R., Eds.; Chemical Analysis 92; Wiley: New York, 1988; pp 3−51.
(19) Teo, B. K. *EXAFS: Basic principles and data analysis*; Inorganic Chemistry Concepts 9; Springer-Verlag: Berlin, 1986.
(20) Mustre de Leon, J.; Rehr, J. J.; Zabinsky, S. I.; Albers, R. C. *Phys. Rev. B* **1991**, *44*, 4146−4156.
(21) Rehr, J. J. *Jpn. J. Appl. Phys., Part 1* **1993**, *32-2*, 8−12.
(22) Rehr, J. J.; Albers, R. C.; Zabinsky, S. I. *Phys. Rev. Lett.* **1992**, *69*, 3397−3400.
(23) Williams, P. *Annu. Rev. Mater. Sci.* **1985**, *15*, 517−448.
(24) Barton, P. B. *Mineral. Soc. Am. Spec. Pap.* **1970**, *3*, 187−198.
(25) Moore, W. J.; Pauling, L. *J. Am. Chem. Soc.* **1941**, *63*, 1392−1394.
(26) Hill, R. J *Acta Crystallogr.* **1985**, *C41*, 1281−1284.
(27) Chisholm-Brause, C. J.; Hayes, K. F.; Roe, A. L.; Brown, G. E., Jr.; Parks, G. A.; Leckie, J. O. *Geochim. Cosmochim. Acta* **1990**, *54*, 1897−1909.
(28) Bargar, J. R.; Brown, G. E., Jr.; Parks, G. A. *Geochim. Cosmochim. Acta* **1997**, *61*, 2617−2637.
(29) Benjamin, M. M.; Leckie, J. O. In *Adsorption of metals at oxide interfaces: effects of the concentrations of adsorbate and competing metals*; Baker, R. A., Ed.; Contaminents and Sediments 2; American Chemical Society: New York, 1980; pp 305−322.
(30) Hayes, K. F.; Leckie, J. O. *J. Colloid Interface Sci.* **1987**, *115*, 564−572.
(31) Waychunas, G. A.; Fuller, C. C.; Davis, J. A. *Stanford Synchrotron Radiation Laboratory Activity Report* 1995; pp 78−80.
(32) Spadini, L.; Manceau, A.; Schindler, P. W.; Charlet, L. *J. Colloid Interface Sci.* **1994**, *168*, 73−86.
(33) Benjamin, M. M. Ph.D. Thesis, Stanford University, Stanford, CA, 1978.
(34) Fornasiero, D.; Fengsheng, L.; Ralston, J.; Smart, R. S. C. *J. Colloid Interface Sci.* **1994**, *164*, 333−344.

(35) Hill, R. J.; Craig, J. R.; Gibbs, G. V. *Phys. Chem. Miner.* **1979**, *4*, 317−339.
(36) Ghose, S. *Acta Crystallogr.* **1964**, *17*, 1051−1057.
(37) Smith, F. G. *Am. Mineral.* **1955**, *40*, 658−675.
(38) Effenberger, H.; Mereiter, K.; Zemann, J. *Z. Kristallogr.* **1981**, *156*, 233−243.
(39) Hang, C.; Simonov, M. A.; Belov, N. V. *Sov. Phys. Crystallogr.* **1970**, *15*, 387−390.
(40) Schnering, H. G. *Z. Anorg. Allg. Chem.* **1964**, *330*, 170−178.
(41) Abrahams, S. C.; Bernstein, J. L. *Acta Crystallogr.* **1969**, *B25*, 1233−1236.
(42) Wildner, M.; Giester, G. *Mineral. and Petrol.* **1988**, *39*, 201−209.
(43) Aurivillius, K.; Stalhandske, C. *Z. Kristallogr.* **1980**, *153*, 121−129.
(44) Wyckoff, R. W. G. *Crystal Structures*; John Wiley & Sons: New York, 1968.
(45) Ksanda, J. *Am. J. Sci.* **1931**, *22*, 131−138.
(46) Borodin, V. L.; Lyutin, V. I.; Ilyukhin, V. V.; Belov, N. V. *Sov. Phys. Dokl.* **1979**, *24*, 226−227.
(47) Noda, Y.; Ohba, S.; Sato, S.; Saito, Y. *Acta Crystallogr.* **1983**, *B39*, 312−317.
(48) Stahl, K. *Z. Kristallogr.* **1974**, *139*, 215−222.

Received for review May 23, 1997. Revised manuscript received October 30, 1997. Accepted January 20, 1998.

ES970453C